IEEE Photonics Journal
An IEEE Photonics Society Publication

Open Access

Performance Optimization by Nonparametric Histogram Estimation for Low Resolution in IMDD-OQAM-OFDM System

Volume 10, Number 4, August 2018

Meihua Bi
Tiancheng Huang
Ling Liu
Xin Miao
Shilin Xiao
Weisheng Hu

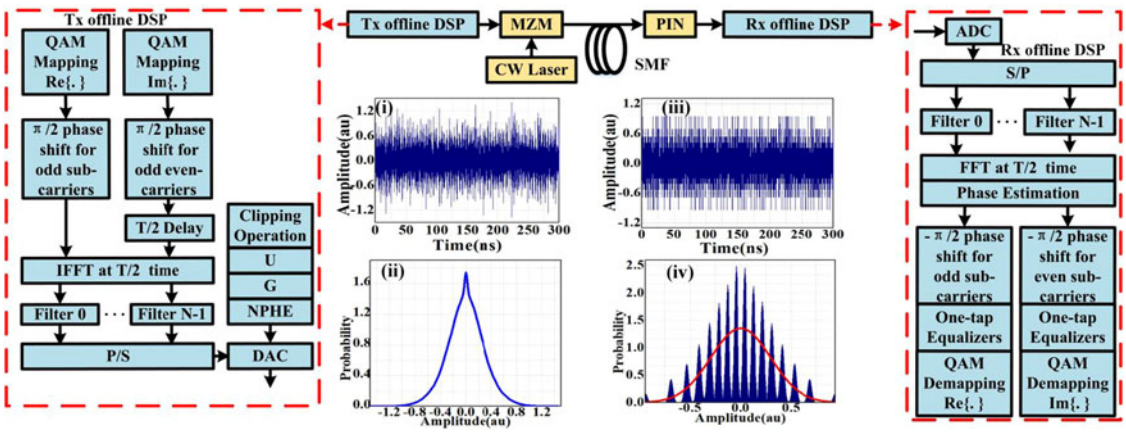

DOI: 10.1109/JPHOT.2018.2848248
1943-0655

Performance Optimization by Nonparametric Histogram Estimation for Low Resolution in IMDD-OQAM-OFDM System

Meihua Bi,[1,2] **Tiancheng Huang**,[2] **Ling Liu**,[2] **Xin Miao**,[2] **Shilin Xiao**,[2] **and Weisheng Hu**[2]

[1]School of Communication Engineering, Hangzhou Dianzi University, Hangzhou 310018, China
[2]State Key Laboratory of Advanced Optical Communication System and Networks, Department of Electronic Engineering,Shanghai Jiao Tong University, Shanghai 200240, China

DOI:10.1109/JPHOT.2018.2848248

Manuscript received May 22, 2018; revised June 10, 2018; accepted June 13, 2018. Date of publication June 18, 2018; date of current version July 4, 2018. This work was supported in part by the Natural Science Foundation of Zhejiang Province under Grant LQ16F050004, and in part by the National Nature Science Fund of China under Grants 61501157, 61775137, 11574068, and 61405051. Corresponding authors: Meihua Bi and Tiancheng Huang (e-mail: bmhua@hdu.edu.cn; 117034910243@sjtu.edu.cn).

Abstract: In this paper, for the first time, we propose a nonparametric histogram estimation (NPHE) scheme for the nonuniform quantization in intensity modulated direct detection with filter bank multicarrier signal to improve system performance. By combining the NPHE scheme and the common nonlinear programming method, the distribution of offset quadrature amplitude modulation based optical orthogonal frequency division multiplexing (OQAM-OFDM) signal is accurately estimated and then it is used to achieve the optimal nonuniform quantization level. In this way, the low-level signal can achieve much more effective digitalizing bits, thereby significantly reducing the quantization noise. The numerical simulation and experiment with 10-Gb/s 16-order OQAM-OFDM signal over 20 km fiber are conducted to further verify the feasibility of our scheme. The results show that our scheme always outperforms the uniform quantization and Gaussian-like nonuniform schemes in terms of the signal to quantization noise ratio, error-vector-magnitudes, and bit error rate. Compared to the conventional method, our scheme also achieves received sensitivity improvement thereby improving the system power budget. So, it can support the low-bit resolution transmission in intensity modulated direct detection-based OQAM-OFDM system.

Index Terms: Nonparametric histogram estimation, nonlinear programming, optical OQAM-OFDM, clipping ratio (CR), the IFFT/FFT bit precision.

1. Introduction

Recently, the emergence of new and developing technologies such as machine learning, social networking and cloud computing cause the rapid growth of traffic throughput and bandwidth demands. To satisfy the requirements of high capacity, asynchronous transmission and considerable spectral efficiency, the Filter Bank based Multicarrier especially with the waveform of the offset quadrature amplitude modulation based optical orthogonal frequency division multiplexing (OQAM-OFDM) has

been widely demonstrated in optical and fiber-wireless communication systems [1]–[6]. Owing to its inherent merits such as high sidelobe suppression ratio, large asynchronous transmission feature, high spectrum efficiency due to the non-requirement of cyclic prefix (CP) and time-frequency domain well-localized pulse shapes, increasing system robustness against inter-carrier interference (ICI) and frequency offset due to lower out-of-band power leakage [6] etc., it has been considered as one of the most promising candidate waveform for intensity modulated direct detection-based (IMDD) optical network transmission system [7]. For the OQAM-OFDM, it is essential to employ a digital-to-analog convertor (DAC) to convert the OQAM-OFDM samples to time-domain waveforms. Apparently, a high bit resolution is desirable for DACs implement, but such a resolution would lead to high power consumption and cost [8], [9]. Besides, based on our previous work [10], it has been verified that, the bit precisions of inverse fast Fourier transform (IFFT) and FFT were also the important limiting factors, and the quantization noise caused by these operations would worsen the system performance.

To deal with these issues, the common amplitude limiting [10], and the encoded peak-to-average power ratio (PAPR) reduction [11], [12] schemes were proposed in IMDD-OFDM system to reduce the bit resolution. However, for these schemes, only few quantization bits were reduced or the limited performance improvements were achieved, and either extra complexity or clipping noises were introduced which would be not suitable for the practical system. In fact, it is easy to get that, the system performance strongly depends on the statistical distribution of the low-bit resolution multicarrier signals' samples, namely the quantization bit of small signal [13]. To deal with this, the nonuniform quantization scheme with the Gaussian-like distribution assumption was proposed in OFDM-based and OQAM-OFDM system [14], [15]. Besides, different from the common OFDM, owing to the filtering effect of OQAM-OFDM signal a non-perfect Gaussian distribution of signal would be achieved, in which a sharp peak would occur on top of gaussian spectrum. In this way, the nonuniform quantization with the Gaussian-like assumption would not be the optimal selection for the IMDD-based OQAM-OFDM system.

Therefore, we propose the nonuniform quantization scheme with a novel nonparametric histogram signal sample estimation to quantify the signals for further reducing the DAC bits with the acceptable system performance in the IMDD-based system. Due to no any requirements of signal distribution in advance, this scheme would be more suitable for the irregular distribution OQAM-OFDM system. In addition, by selecting the appropriate kernel density function and window width, the OQAM-OFDM signals' distribution can be accurately estimated. Then, by combining nonlinear programming technique, the optimal nonuniform-distributed discrete output levels of OQAM-OFDM signal are achieved. In this way, more effective quantization bits can be assigned to the small OQAM-OFDM signals hence reducing quantization noise and improving system performance. To verify the feasibility of this scheme, the simulation (the commercial software OptiSystem 13) and experiment with the 10-Gb/s 16-OQAM-OFDM signal for 20-km fiber transmission with different DACs and IFFT/FFT bit resolution is constructed. The simulation results show that, for the 4-bit and 6-bit DAC case, $\sim$9.1 dB and $\sim$3.4 dB receiver sensitivity improvement @BER $=$ 3.8e-3 can be achieved in comparison with the common uniform scheme, and compared to the Gaussian-like distribution nonuniform method, our scheme also demonstrates better performance. Meanwhile, by experiment, we can easily get that, our scheme with the 5-bit DAC can achieve the same performance as the common scheme with 7-bit DAC. Therefore, our demonstrated scheme can be considered as a promising way to improve the performance of the IMDD-based OQAM-OFDM optical system, especially with the low-bit resolution DAC.

2. Principle

Firstly, we give the schematic diagram of IMDD OQAM-OFDM system to further illustrate the proposed NPHE scheme as shown in Fig. 1, which includes optical OQAM-OFDM transmitter, fiber transmission link and OQAM-OFDM receiver. At the transmitter, as configured in our previous work [15], the pseudo-random binary sequence (PRBS) data is firstly mapped into M-order offset quadrature amplitude modulation (M-OQAM) complex symbols, then is divided into the odd and

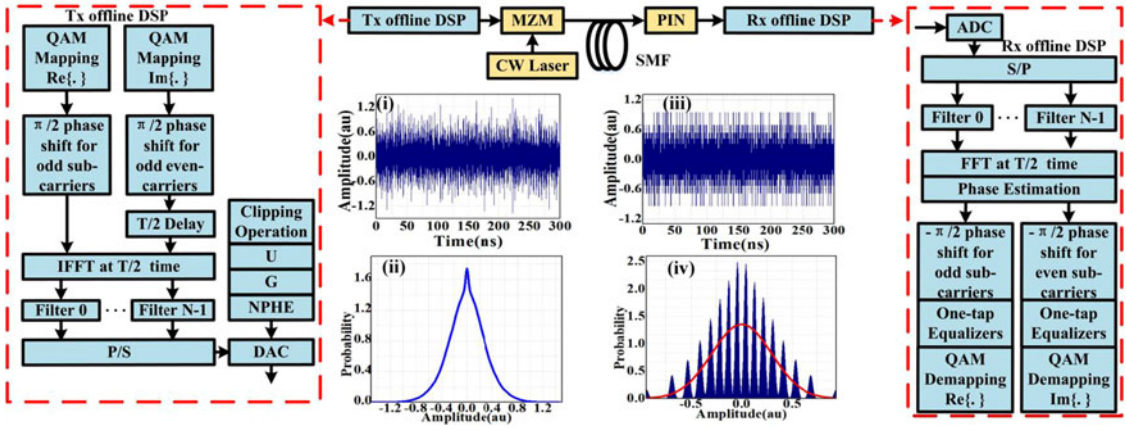

Fig. 1. (a) Schematic structure of the optical IMDD-based OQAM-OFDM system. Inserts (i) and (ii) are the waveforms and the distribution profile of the OQAM-OFDM samples, inserts (iii) and (iv) are the waveforms and distribution profile of 4-bit NPHE-based nonuniform quantization DAC samples. U: the common uniform quantization, G: the Gaussian-like estimation nonuniform quantization.

even subcarriers modules and phase shifted by 90 degrees. For the even subcarriers, they are delayed by a half symbol period T/2. After that, these two modules data are fed to the 128-point IFFT module whose bit precision varies from m = 3 to 17 bits at T/2-time interval. After IFFT, the in-phase and quadrature tributary samples are injected into the specially designed finite impulse response (FIR) filters [16] for pulse shaping. Then, after the parallel-to-serial (P/S) conversion, the data is clipped and scaled to interface with a k-bit DAC to generate the electrical OQAM-OFDM signals. In the DAC module, for sake of comparative analysis, the Gaussian-like nonuniform, the uniform and our proposed NPHE-based nonuniform quantization are also involved. Based on our previous work [15], the quantization noise e_q is the key factor which is needed be minimized, and it is related to signal's probability density function (PDF) *f(x)* given by,

$$e_q = \int_{-\infty}^{+\infty} (x - x_q)^2 f(x) dx \tag{1}$$

Where, x_q is the discrete output of the digital sample x. From this equalization, we can easily get that, the e_q depends strongly on the OQAM-OFDM signal's distribution *f(x)* and that of the output level of DAC x_q. Thus, we give the electronical waveforms and its PDF diagram of OQAM-OFDM signal as shown in insert (i) and (ii) of Fig. 1. It is observed that, the PDF of OQAM-OFDM signal has a large sharp value during the region of small distribution. Such distribution means that OQAM-OFDM signal cannot be considered as a Gaussian profile, and it has most waveforms samples constrained in this small amplitude region. Meanwhile, *f(x)* of the signal is the same for symmetric positive and negative levels as shown in this figure. In this way, Eq. (1) can be rewritten as Eq. (2).

$$e_q \approx 2 \times \int_{0}^{+\infty} (x - x_q)^2 f(x) dx \tag{2}$$

To estimate the distribution of OQAM-OFDM signal, the NPHE scheme is employed. For this scheme, the sample space is firstly divided into a number of bins, and the points in the training data approximate the density at the center of each bin. The PDF of signal quantized by NPHE scheme *p(x)* is

$$\int_X p(x)dx = 1,\ p(x) = \frac{\text{Number of observations in the samebin}_x}{\text{N} \times \text{Width of bin}_x} \tag{3}$$

Where N is the number of samples. In Eq. (3), X represents the signals' amplitude region. To summarize, the procedure of nonparametric histogram estimation is constructed as follows. Step 1,

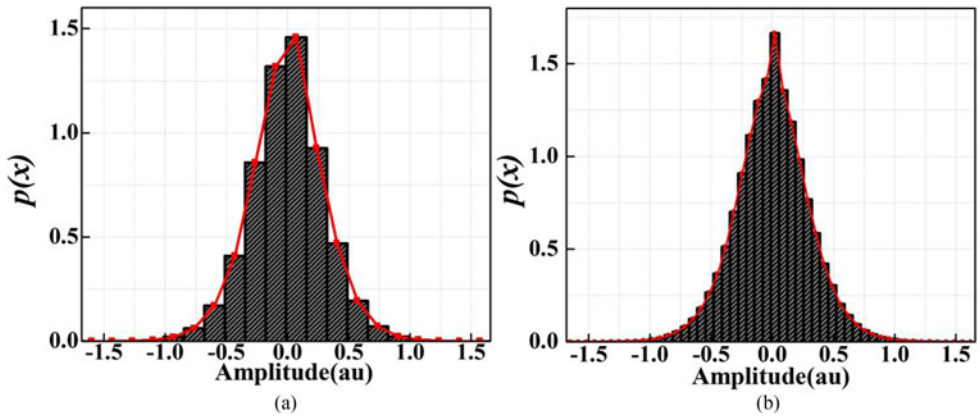

Fig. 2. The PDF profiles of non-parametric histogram estimation method with (a) 20 bins and (b) 50 bins.

Determine the range of bin due to the range of signals' value and divide the entire range into m bins which are consecutive and have the same width. Here, the width can be denoted as w = (max(X)-min(X))/m. Step 2, Initialize the height of each bin to zero and calculate the number of the samples which is given as N. Step 3, Put one sample point into the corresponding bin and the height of this bin would add 1/N. Step 4, Repeat step 3 for all the sample points, then each height of each bin divided by w to guarantee total probability equals one. Step 5, link the midpoint of each bin which is depicted as p(x). In this way, an approximate probability density function p(x) can be obtained. Here, the histogram method can provide an approximate density distribution estimation for the sample data. In fact, the bin width and the starting position of the first bin are two valid arguments of the histogram method. In this paper, the starting position of first bin is ascertained due to the range of signals' value, hence histogram bin size is a key factor for acquiring accurate *f(x)*. Further, we plot the distribution profile of signals with NPHE method as shown in Fig. 2, in which the number of bins is set to 20 and 50 respectively. Here, the bar is the NPHE-based estimated signals and the line is referred as to the approximate PDF of original signals. From these figures, we can see that the small bin width can fit fine details of distribution, while the large one cannot emulate the details of distribution. Whereas, in practical system, the extremely small bin width would bring not only high calculation complexity but also abrupt jagged changes at bin boundaries due to a small amount of data in each bin. Therefore, the smaller bin width might overfit and lager one might underfit. For this consideration, by the simulated analysis, we can get that, one thousand bins are large enough to achieve the trade-off between system performance and complexity.

For the NPHE-based estimated OQAM-OFDM signals, the properly DAC with output levels took into account the signals' distribution can better exploit all available signal levels thereby reducing the quantization noise namely improving the signal quantization noise ratio (SQNR). Here, the nonuniform quantization scheme is selected, and the corresponding quantization outputs of n-bit DAC with 2^n discrete output level can be expressed as:

$$x_q(x) = \begin{cases} \frac{q_{2^{n-1}-1}+q_{2^{n-1}}}{2}, x \geq q_{2^{n-1}-1} \\ \vdots \\ \frac{q_1}{2}, q_1 >\geq 0 \\ \frac{q_{-1}}{2}, q_{-1} \leq x < 0 \\ \vdots \\ \frac{q_{-(2^{n-1}-1)}+q_{-2^{n-1}}}{2}, x \leq q_{-(2^{n-1}-1)} \end{cases} \tag{4}$$

where, the $[q_{-(2^{n-1}-1)} \ldots q_{-2}, q_{-1}, 0, q_1, q_2 \ldots q_{2^{n-1}-1}]$ are the values of signal quantization interval endpoint, which is more densely assigned for the middle value in the nonuniform. In this way,

the output of OQAM-OFDM by DAC would achieve the significantly benefits for its waveforms mainly concentrated in small amplitude regions, resulting in the quantification noise reduction of the whole signals. To describe this principle, the mathematical derivation is given as following. Due to the output levels of OQAM-OFDM signals are symmetric for the negative and positive parts, the positive part of DAC is selected to be analyzed. Based on this assumption, by substituting Eq. (4) into Eq. (2), we define the formula$h(x) = \int_0^x tf(t)dt$ and $g(x) = \int_0^x f(t)dt$ for simplicity, the detailed derivation is presented in the appendix. Then, the new expression of e_q can be given as,

$$\begin{aligned} e_q \propto & \frac{(0-q_2)\times(0+q_2+2q_1)}{4}g(q_1) + \frac{(q_1-q_3)\times(q_1+q_3+2q_2)}{4} \\ & g(q_2) + \ldots + \frac{(q_{2^{n-1}-2}-q_{2^{n-1}})\times(q_{2^{n-1}-2}+q_{2^{n-1}}+2q_{2^{n-1}-1})}{4}g(q_{2^{n-1}-1}) \\ & + \frac{(q_{2^{n-1}-1}+q_{2^{n-1}})^2}{4}g(+\infty) - [(0-q_2)h(q_1) + (q_1-q_3)h(q_2) + \ldots \\ & + (q_{2^{n-1}-2}-q_{2^{n-1}})h(q_{2^{n-1}-1}) + (q_{2^{n-1}}+q_{2^{n-1}-1})h(+\infty)] \end{aligned} \tag{5}$$

From Eq. (5), the quantization noises turn out to be a function of the discrete output of $[q_1, q_2 \ldots q_{2^{n-1}-1}]$. So, to minimize the e_q, as in our previous work [15], a common nonlinear programming method is used by finding out the suitable discrete output levels $[\frac{q_1}{2}, \frac{q_1+q_2}{2} \ldots \frac{q_{2^{n-1}-1}+q_{2^{n-1}}}{2}]$, which is presented as,

$$\begin{aligned} & \min e_q \\ & s.t. \quad q_{j+1} > q_j > 0, j = 1, \ldots, 2^{n-1}-1 \\ & \qquad q_{2^{n-1}-1}+q_{2^{n-1}} = 2 \times CRn \times \sigma_s \end{aligned} \tag{6}$$

Here, the PDF of the OQAM-OFDM signals can be achieved by the NPHE scheme and the signals' standard derivation σ_s is calculated by the training data. In this Eq. (6), minimizing the e_q from the Eq. (5) is our goal. Moreover, from the basic principle of quantization process and the range of sampled signals, we can easily get two constraint conditions as presented in Eq. (6). As defined in the previous reports [10], [15], the *CR* is introduced to imitate the clipping operation of DAC-modules, which is defined as the ratio of the maximum to the average output power and is used to reduce the peak-to-average power ratio (PAPR) of OQAM-OFDM signals. Here, *CRn* is the *CR* for n-bit DAC, which is normalized to σ_s and is inversely proportional to the level of PAPR reduction brought by clipping. As implemented in our work [15], with the help of the Eq. (6) , we conduct the simulation system by MATLAB to achieve the optimized $[q_1, q_2 \ldots q_{2^{n-1}-1}]$, which can minimize the quantization noise for the low-bit DAC with the given *CRn*.

As shown in Fig. 1, throughout the DAC processing, the low-bit electronical OQAM-OFDM signals can be generated, and they are used to drive the Mach-Zehnder modulator (MZM) working at linear modulation region. A 1550-nm continuous wave (CW) as the optical carrier is injected into MZM. The optical OQAM-OFDM signals with ∼7.5 dBm power are transmitted into the 20-km single mode fiber (SMF). At the receiver, the optical OQAM-OFDM signals after fiber transmission are injected into a linear photoelectric detector for recovering the electrical signals, which are sampled by oscilloscope for further offline processing. For this process, an emulated ADC is used to construct the bit resolution, which varies from 4bit to 10bit. Then, the sampled signals are transmitted into the FFT module with 3∼17-bit precision. These results of different bit precision and bit resolution could be considered as a guideline for designing real time optical OQAM-OFDM systems. At last, the signals are injected into the one-tap equalization module for further recovering the data. Here, the fixed-point models based on the Cooley-Tukey radix-2 algorithm [17] is used for the FFT and IFFT calculation. In addition, for a DAC even with nonuniform quantization, only limited number of discrete levels are output for its limited bit resolution. In addition, for the low-bit case, strong quantization noise can be occurred which is detrimental for system performance [18]. An example

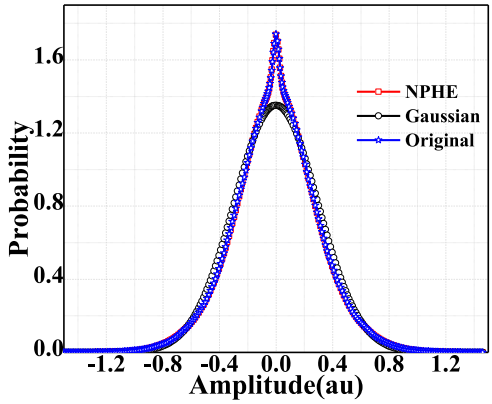

Fig. 3. The PDF diagram of OQAM-OFDM signals.

TABLE 1
Comparison of Two Methods

	R-square	SSE	RMSE
Gaussian	0.9921	1.744	0.04218
NPHE	1	0.009215	0.003048

for the output waveform of the OQAM-OFDM signals with 4-bit non-uniform quantization DAC is presented in insert (iii), and its pdf profile is given as in insert (iv) of Fig. 1.

3. Simulation and Experimental Verification

In this section, to verify the validity of our proposed scheme, we conduct the 10-Gb/s IMDD-based 16-OQAM-OFDM transmission over 20-km standard single mode fiber (SMF) simulaiton and experimental system. Besides, for the sake of comparative analysis, uniform quantization and Gaussian-like profile estimation non-uniform quantization are also involved in this setup. In addition, to further verify the feasibility of our scheme, we evaluate the effect IFFT/FFT bit precision and the *CRn* for different bit DAC/ADC on performance.

3.1 Simulation and Results Analysis

Firstly, to verify the feasibility of NPHE scheme, we give the probability density function (PDF) of the original OQAM-OFDM signals, the NPHE method and the Gaussian-like estimation are also presented, which is shown in Fig. 3, in which the ∼65535 OQAM-OFDM symbol with 128-point FFT is configurated. For the original OQAM-OFDM signals, an obvious peak occurs which can be attributed to the filter effect of filter banks. Compared to the common Gaussian distribution signals, such shape means that larger probability samples would locate in the small signals region. Besides, in this figure, the NPHE scheme almost completely keep pace with the real distribution of OQAM-OFDM signals. While the Gaussian-like method is unable to fit in with such sharp profile. Therefore, the Gaussian-like estimation scheme cannot be directly used for OQAM-OFDM-based system.

Moreover, to further verify the NPHE scheme, we calculated the similarity degree R-square [19], the sum of squares due to error (SSE) [20] and root mean squared error (RMSE) [21] for the original and estimated OQAM-OFDM signal, which is demonstrated in Table 1. Here, ∼65535 OQAM-OFDM symbols are employed, and 1000 bins is configured for the NPHE scheme. From the results as in table, we can easily get that, compared to the Gaussian scheme, our proposed scheme can

TABLE 2
Simulation Parameters

Sampling rate	10 GSa/s
Sequence length	524288
Symbols per bit	1
Constellation mapping	16-OQAM(4-bit)
Subcarrier number	128
Design of filter	Root-raised-cosine(SRRC)with memory depth of 6
Laser frequency	193.1 THz
Laser Power	10 dBm
Laser linewidth	10 MHz
Vpi of MZM	4.6V
Extinction Ratio of MZM	25dB
Insert loss of MZM	7dB
Fiber attenuation	0.2dB/km
Fiber dispersion	16.75 ps/nm/km
PIN responsivity	1 A/W
ADC resolution	Infinite
CRn	1-5

achieve the larger R-square value and its SSE and RMSE values would gradually decrease and tend to zero, which further verify the high estimation accuracy of our scheme.

Based on the configuration of Fig. 1, using the commercial software Optisystem 13 and MATLAB programming, we perform the system simulation to further investigate the NPHE-based nonuniform quantization method implemented in IMDD-OQAM-OFDM transmission system. Here, to make results be consisted with the experiment in 3.2, all parameter settings of system devices (including CW, MZM, *et al.*) are adjusted to achieve the best fit with experiment and we use the highest precision of IFFT/FFT in MATLAB (double precision floating point) to improve the credibility of numerical analysis. The corresponding simulation parameters are given in the Table 2. The OQAM-OFDM samples are generated by the module of this optical software. And, the clipping operation is given in the MATLAB processing for various *CRn* which would limit the signals' amplitude range. Meanwhile, to make the trade-off between the system performance and the PAPR of OQAM-OFDM signals, the $CRn = 3$ is employed for 4-bit and 5-bit DAC, and $CRn = 4$ for the 6-bit, 8bit and 10-bit DACs case.

For a fixed *CRn*, the distribution of OQAM-OFDM signals is determined by the NPHE method, then is injected into the nonuniform quantization module by selecting the optimal quantization level. In this case, we can easily calculate the SQNR of IMDD-based OQAM-OFDM signals with 4-bit and 5-bit resolutions, which is shown in Fig. 4(a). For comparative analysis, the common uniform quantization and Gaussian-like estimation nonuniform quantization are presented in this figure. And, the zoom-in details for the NPHE-based scheme and Gaussian-like estimation nonuniform quantization method with the same bit resolution are depicted in the inserts (i) and (ii). It is presented that, our proposed method always outperforms the Gaussian-like estimation nonuniform quantization and common uniform quantization schemes, and the outperformance is more apparent with the increasing *CRn*. At the same time, with the increase of bit resolution, the optimum *CRn* becomes larger. Compared to the Gaussian-like estimation nonuniform quantization and common uniform quantization schemes, the SQNR can achieve 0.72 dB and 3.72 dB improvement under 4-bit resolution, 0.55 dB and 3.88 dB improvement under 5-bit resolution respectively with the optimum *CRn* case. While the *CRn* is lower than a certain value, almost the same SQNR performance can be obtained for these three schemes. In addition, we also give the SQNR versus the *CRn* with the high-bits DAC as shown in Fig. 4(b). From this figure, it is observed that, compared to the other schemes, our scheme also

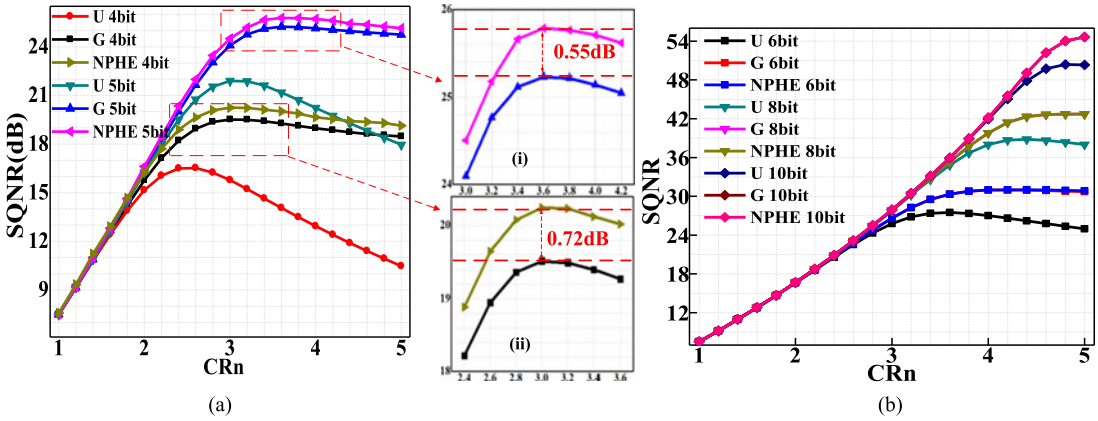

Fig. 4. Calculated SQNR versus different DAC bit resolution and *CRn* (Normalized to σ_s) for (a) 4-bit and 5-bit; (b) 6-bit, 8-bit and 10-bit resolutions.

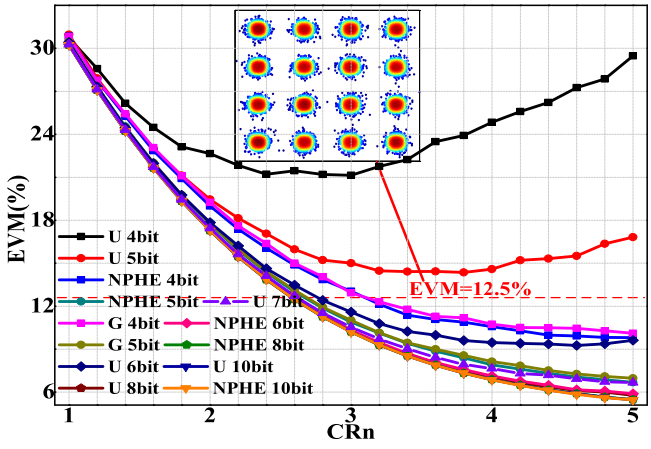

Fig. 5. EVM versus different DAC bit resolution and *CRn* (Normalized to σ_s).

achieves the largest SQNR improvement with the increase of the bit resolution. And with the bit resolution increasing, the difference between the Gaussian-like estimation nonuniform quantization scheme and our scheme become smaller and smaller. These results can effectively verify that, our scheme can be used for IMDD-OQAM-OFDM system, especially with the low-bit resolution case.

Then, the EVM of different quantization methods are also calculated and measured as depicted in Fig. 5. The EVM performance of NPHE is always better than the other schemes. Specifically, at the *CRn* of 4, NPHE scheme can bring the improvements of 14.3%, 6.7% and 2.3% in comparison with the common uniform quantization scheme under 4-bit, 5-bit and 6-bit resolutions, respectively, and brings the improvements of 0.6% and 0.3% under 4-bit and 5-bit resolutions, respectively compared to Gaussian-like estimation nonuniform quantization method.

In addition, the effect of IFFT/FFT bit precision on optical IMDD-based OQAM-OFDM with NPHE-based quantization system is also studied to provide a guide for designing FPGA that contains IFFT/FFT modules. Fig. 6(a) gives the SQNR in terms of the IFFT/FFT precision without any quantization and clipping operation. The gradient of SQNR versus IFFT/FFT precision is 6 dB/bit. Fig. 6 (b) and (c) depict the SQNR performance of NPHE as a function of IFFT and FFT bit precisions respectively with different bit resolutions for the optimum CRn. Here, for IFFT case, the different DAC bits with the resolutions from 4 bit to 10 bit (ADC is assumed that enough bits are configured) is used to evaluate the performance for different bit precision of IFFT as shown in Fig. 6(b). Similarly, for FFT case, the ADC with the resolutions from 4bit to 10bit (DAC is assumed that enough bits are configured) is employed as shown in Fig. 6(c) [22]. Moreover, in other paragraph,

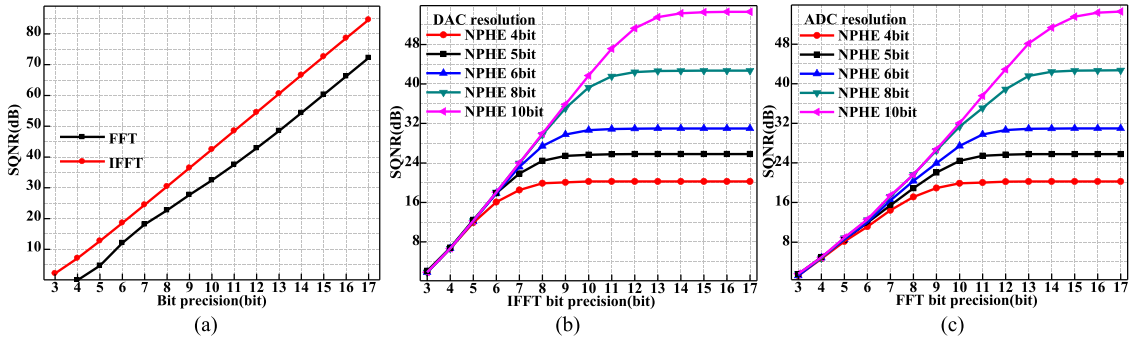

Fig. 6. (a) SQNR versus IFFT/FFT bit precision without any quantization and clipping effects; SQNR versus (b) IFFT and (c) FFT bit precision with 16-OQAM in IMDD optical link.

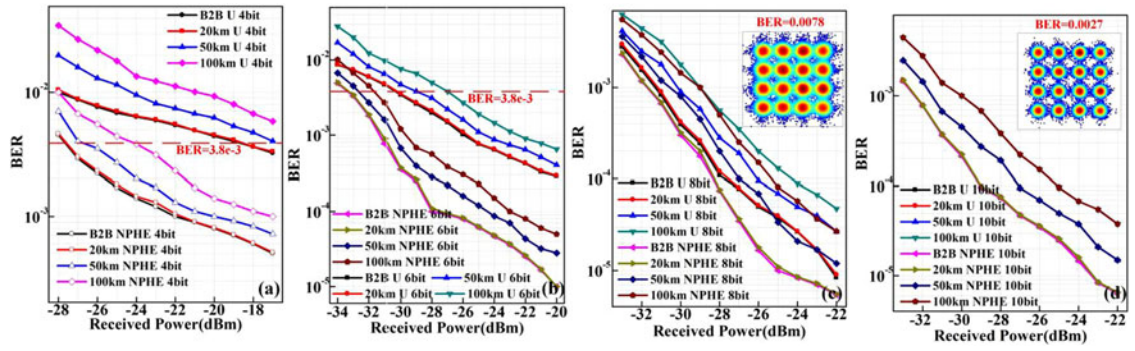

Fig. 7. BER versus received optical power @B2B, 20-km, 50-km and 100-km SMF for (a) 4-bit DAC, (b) 6-bit DAC, (c) 8-bit DAC and (d) 10-bit DAC.

only the comparison of DAC results and the analysis of DAC (ADC is assumed that enough bits are configured) are given [14]. Besides, it is noted that, two regions can be split for these two figures. One of them is IFFT/FFT bit precision limited region where the system performance is restricted by the IFFT/FFT precision. And, with the increase of DAC/ADC bit resolution, almost no any obvious SQNR improvement is observed, while for the increasing IFFT/FFT bit precision will benefit the SQNR. The other is DAC/ADC bit resolution limited region where the system performance is insensible to the increase of IFFT/FFT bit precision.

The BER curves of back-to-back (B2B), 20-km, 50-km and 100-km transmission cases are illustrated in Fig. 7. Due to the small BER difference between our scheme and the Gaussian-like estimation nonuniform quantization method, only our proposed NPHE scheme is plotted in these figures. The received sensitivity curves with the 4-bit, 6-bit, 8-bit and 10-bit DACs is illustrated in Fig. 7(a), (b), (c) and (d) respectively. The results show that the performance under B2B and 20-km cases are similar and the performance becomes worse under 50-km and 100-km cases. It is observed that conventional 4-bit DAC cannot achieve forward error correction (FEC) threshold of BER $=$ 3.8e-3, while our scheme can achieve with 4-bit and 6-bit DACs at the received optical power of ~ -22 dBm and ~ -31 dBm, respectively. Compared to the common uniform quantization scheme, our scheme can achieve $\sim$9.1-dB and $\sim$3.4-dB sensitivity improvements @BER $=$ 3.8e-3 for 4-bit and 6-bit DAC, respectively. In contrast to our previous work [15], we can conclude that our scheme can achieve $\sim$0.4-dB sensitivity improvement @BER $=$ 3.8e-3 for 4-bit resolution in comparison with Gaussian-like estimation nonuniform quantization method. Moreover, compared to common uniform quantization method, our scheme can achieve $\sim$0.5-dB sensitivity improvements @BER $=$ 1e-3 in the 8-bit DAC case. And when the bit resolution approaches 10, all the curves overlap. In brief, our scheme can immensely improve the performance in the low bit resolution case compared with the common uniform quantization scheme. Moreover, in the high bit resolution case,

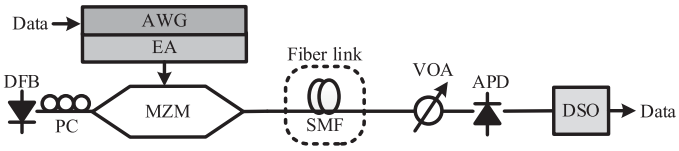

Fig. 8. Experimental schematic setup of our proposed scheme.

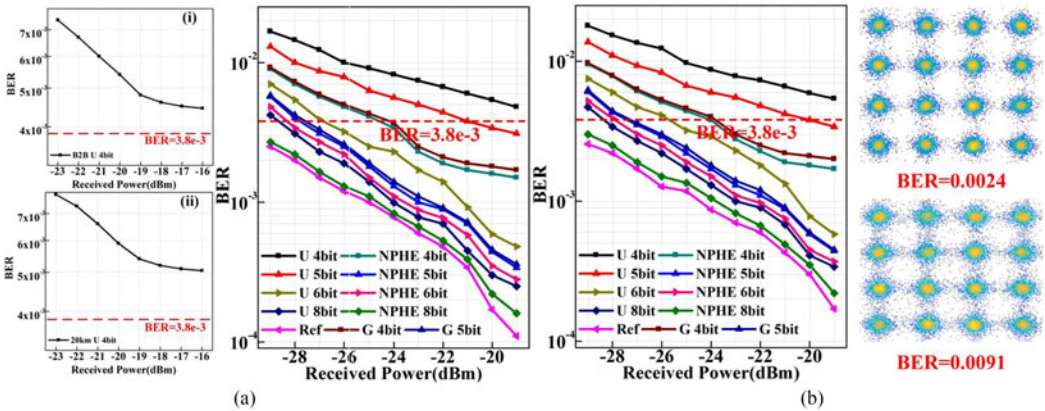

Fig. 9. Experimentally measured BER curves versus received optical power at (a) B2B condition and after (b) 20-km SMF transmission for all DAC, inserts (i) and (ii) are the B2B and 20-km fiber BER curves for U scheme with the 4-bit DAC.

our proposed scheme results in limited improvements of BER and EVM due to the advancement of modulation-demodulation and the sufficient quantization levels.

3.2 Experimental Setup and Results Discussion

This section gives the further verification by the proof-of-concept experiment. And, the experiment schematic setup is depicted in Fig. 8. The OQAM-OFDM samples can be generated offline by MATLAB following the same procedures shown in Fig. 1(a). 16-QAM mapping is applied to the OQAM-OFDM signals. A MZM biased at the quadrature point of its transmission curve is employed to modulate the CW light wave from a DFB laser at 1550 nm. Here, the Vpi of MZM is 4.6 V and the extinction ratio of MZM is 25 dB, its insert loss is $\sim$7 dB. And the electrical OQAM-OFDM signals are output by the arbitrary waveform generator (AWG, Tektronix AWG7122C) varying form -1 V to 1 V with a 10-GSa/s sampling rate. We used a 10-bit resolution AWG. The AWG actually is able to output 1024 electrical discrete levels spread over the dynamic range. When in the 4-bit case, among those 1024 levels, only sixteen levels are chosen and utilized to perform as a distributed 4-bit DAC according to the signal's distribution [14]. The mapping from continuous distribution to sixteen-level distribution is also achieved by offline program, after the mapping, the final data for DAC is imported to AWG. Then, we employ an electrical amplifier (EA) to boost the OQAM-OFDM signals to match with the linear region of the MZM. Next, the modulated light is injected into the SMF. After SMF transmission, the received optical signal is attenuated by a variable optical attenuator (VOA) to change the received optical power and then detected by a specifically-designed APD [23]. At last, we use a digital storage oscilloscope (DSO) to capture the OQAM-OFDM signals. The DSP post-processing is realized offline by MATLAB to accomplish channel estimation, FFT, one-tap equalization, constellation-symbol demapping and BER counting.

The experimental BER curves in both B2B and 20-km transmission case are illustrated in Fig. 9. The results of "Ref" are processed by full bit-resolution (10-bit resolution in this experiment) DACs, thus the BER performance is the best. The experimental results agree very well with the simulation results, verifying that our proposed scheme can reliably improve the performance of the IMDD-based OQAM-OFDM system. In the condition of low bit resolution, the major system performance loss is

caused by intense quantization noise. Therefore, NPHE scheme outperforms the common uniform quantization scheme obviously. This occurs, because the limited quantization levels obtained by our scheme fits the characteristic of OQAM-OFDM signals faultlessly more preferably in comparison with the common uniform quantization scheme. NPHE method can achieve the ideal BER level for 4-bit and 5-bit DACs at the received optical power of ~ -24 dBm and ~ -27.3 dBm @BER $=$ 3.8e-3, respectively. With the increase of bit resolution, the system performance obtained by NPHE method approaches the common uniform quantization method gradually. Besides, as for the 4-bit DAC case, the insert (i) and (ii) depict that the BER curves hardly reach the performance BER $=$ 3.8e-3 with the increasing received power. This can be attributed to that the high quantization noise induced by the large quantization interval for the uniform quantization scheme. While, using our scheme, as in Fig. 9(a) and (b), even with 4-bit case, the BER performance is significantly improved, thereby increasing the system power budget. This can further verify that, our proposed NPHE scheme can be considered a promising scheme to improve system performance, especially for low-bit DAC.

4. Conclusions

For the first time, the DAC optimization scheme based on nonparametric histogram estimation, which employs the best combination of discrete output levels of OQAM-OFDM signals, is investigated. The quantization noise is mitigated immensely and SQNR, EVM and BER are improved markedly in the low bit resolution case. In the simulation, over $\sim$3.72-dB and 3.88-dB SQNR improvements with 4-bit and 5-bit DAC are achieved, respectively. The BER performance of 4-bit DACs based on our scheme is evaluated by simulation and further confirmed experiment achieving BER of 3.8e-3 for OQAM-OFDM signals with ~ -27.7-dBm and ~ -24-dBm power, respectively. It is worthy to note that the gap of system performance between NPHE scheme and the common uniform quantization scheme will get smaller with the increase of bit resolution. Both simulation and the proof-of-concept experiment validate the feasibility of NPHE scheme for OQAM-OFDM signals. For giving more feasible analysis, we also provide the impact of IFFT/FFT bit precision on system performance, which can be a guide for IFFT/FFT module in FPGA design. In summary, NPHE scheme can be used to improve the system performance in the IMDD-based OQAM-OFDM system compared to common uniform scheme with the same DAC bit resolution, especially for a low-bit DAC.

Appendix

Firstly, by substituting Eq. (4) into Eq. (2) of paper, the Eq. (2) of manuscript can be split into 2n-1 parts,

$$e_q \propto \int_0^{q_1} \left(x^2 - q_1 x + \frac{{q_1}^2}{4}\right) f(x)dx + \int_{q_1}^{q_2} \left(x^2 - (q_1+q_2)x + \frac{(q_1+q_2)^2}{4}\right) f(x)dx + \ldots + \int_{q_{2^{n-1}-1}}^{+\infty} \left(x^2 - (q_{2^{n-1}-1} + q_{2^{n-1}})x + \frac{(q_{2^{n-1}-1} + q_{2^{n-1}})^2}{4}\right) f(x)dx \tag{1-1}$$

The Eq. (1-1) can be formalised, and it can be presented as Eq. (1-2),

$$\begin{aligned} e_q \propto & \int_0^{q_1} x^2 f(x)dx + \int_{q_1}^{q_2} x^2 f(x)dx + \ldots + \int_{q_{2^{n-1}-1}}^{+\infty} x^2 f(x)dx \\ & + \int_0^{q_1} \frac{{q_1}^2}{4} f(x)dx - \int_0^{q_1} \frac{(q_1+q_2)^2}{4} f(x)dx + \int_0^{q_1} \frac{(q_1+q_2)^2}{4} f(x)dx + \int_{q_1}^{q_2} \frac{(q_1+q_2)^2}{4} f(x)dx + \ldots \\ & - \int_0^{q_1} q_1 x f(x)dx + \int_0^{q_1} (q_1+q_2) x f(x)dx - \int_0^{q_1} (q_1+q_2) x f(x)dx - \int_{q_1}^{q_2} (q_1+q_2) x f(x)dx - \ldots \end{aligned} \tag{1-2}$$

After merging the similar terms, Eq. (1-2) can be written as,

$$e_q \propto \int_0^{+\infty} x^2 f(x)dx + \int_0^{q_1} \frac{{q_1}^2 - (q_1+q_2)^2}{4} f(x)dx + \ldots + \int_0^{+\infty} \frac{(q_{2^{n-1}-1}+q_{2^{n-1}})^2}{4} f(x)dx$$
$$- \int_0^{q_1} (q_1 - q_1 - q_2) x f(x)dx - \int_0^{q_2} (q_1+q_2-q_2-q_3) x f(x)dx - \ldots - \int_0^{+\infty} (q_{2^{n-1}-1}+q_{2^{n-1}}) x f(x)dx \quad (1\text{-}3)$$

where, the format $\int_0^{+\infty} x^2 f(x)dx$ can be considered as a constant for its fixed f(x) and integral interval. And, for simplicity, we define the formula $g(x) = \int_0^x f(t)dt$ and $h(x) = \int_0^x tf(t)dt$. In this way, the new expression of e_q can be given as,

$$e_q \propto \frac{(0+q_1-q_1-q_2)\times(0+q_1+q_1+q_2)}{4} g(q_1) + \frac{(q_1+q_2-q_2-q_3)\times(q_1+q_2+q_2+q_3)}{4} g(q_2)$$
$$+ \ldots + \frac{(q_{2^{n-1}-2}+q_{2^{n-1}-1}-q_{2^{n-1}-1}-q_{2^{n-1}})\times(q_{2^{n-1}-2}+q_{2^{n-1}-1}+q_{2^{n-1}-1}+q_{2^{n-1}})}{4} g(q_{2^{n-1}-1})$$
$$+ \frac{(q_{2^{n-1}-1}+q_{2^{n-1}})^2}{4} g(+\infty) - [(0+q_1-q_1-q_2)h(q_1) + (q_1+q_2-q_2-q_3)h(q_2) + \ldots$$
$$+ (q_{2^{n-1}-2}+q_{2^{n-1}-1}-q_{2^{n-1}-1}-q_{2^{n-1}})h(q_{2^{n-1}-1}) + (q_{2^{n-1}}+q_{2^{n-1}-1})h(+\infty)] \quad (1\text{-}4)$$

Finally, the Eq. (1-4) can be further simplified and it is given as the Eq. (1-5),

$$e_q \propto \frac{(0-q_2)\times(0+q_2+2q_1)}{4} g(q_1) + \frac{(q_1-q_3)\times(q_1+q_3+2q_2)}{4} g(q_2) + \ldots$$
$$+ \frac{(q_{2^{n-1}-2}-q_{2^{n-1}})\times(q_{2^{n-1}-2}+q_{2^{n-1}}+2q_{2^{n-1}-1})}{4} g(q_{2^{n-1}-1}) + \frac{(q_{2^{n-1}-1}+q_{2^{n-1}})^2}{4} g(+\infty)$$
$$- [(0-q_2)h(q_1) + (q_1-q_3)h(q_2) + \ldots + (q_{2^{n-1}-2}-q_{2^{n-1}})h(q_{2^{n-1}-1}) + (q_{2^{n-1}}+q_{2^{n-1}-1})h(+\infty)] \quad (1\text{-}5)$$

References

[1] Z. Zheng, D. Wang, X. Zhu, X. Lv, K. Zou, and Y. Zhu, "Orthogonal-band-multiplexed offset-QAM optical superchannel generation and coherent detection," *Sci. Rep.*, vol. 5, Dec. 2015, Art. no. 17891.

[2] Y. Yu, P. D. Townsend, and J. Zhao, "Equalization of dispersion-induced crosstalk in optical offset-QAM OFDM systems," *IEEE Photon. Technol. Lett.*, vol. 7, no. 28, pp. 782–785, Feb. 2016.

[3] S. Y. Jung, S. M. Jung, H. J. Park, and S. K. Han, "Mitigation of timing offset effect in IM/DD based OFDMA-PON uplink multiple access," *Opt. Express*, vol. 23, no. 11, pp. 13889–13898, May 2015.

[4] C. Liu, L. Deng, J. He, D. Li, S. Fu, and M. Tang, "Non-orthogonal multiple access based on SCMA and OFDM/OQAM techniques in bidirectional RoF system," in *Proc. Opt. Fiber Commun. Conf.*, Mar. 2017, paper W2A.41.

[5] A. Saljoghei, F. A. Gutiérrez, P. Perry, D. Venkitesh, R. D. Koipillai, and L. P. Barry, "Experimental comparison of OQAM-OFDM and OFDM for multiple access uplink PON," *J. Lightw. Technol.*, vol. 35, no. 4, pp. 1595–1604, May 2017.

[6] J. He, J. Shi, R. Deng, and L. Chen, "Experimental demonstration of OFDM/OQAM transmission with DFT-based channel estimation for visible laser light communications," *Proc.SPIE*, vol. 10395, 2017, Art. no. 103950Z.

[7] M. Xu *et al.*, "FBMC in next-generation mobile fronthaul networks with centralized pre-equalization," *IEEE Photon. Technol. Lett.*, vol. 28, no. 18, pp. 1912–1915, Sep. 2016.

[8] C. Laperle and M. O.'Sullivan, "Advances in high-speed DACs, ADCs, and DSP for optical coherent transceivers," *J. Lightw. Technol.*, vol. 32, no. 4, pp. 629–643, Feb. 2014.

[9] C. Schmidt *et al.*, "Bandwidth enhancement for an optical access link by using a frequency interleaved DAC," in *Proc. Opt. Fiber Commun. Conf.*, Mar. 2018, paper W4G.2.

[10] M. Bi *et al.*, "Study of FFT/IFFT precision in optical OQAM-OFDM system with limited resolution DAC/ADC," in *Proc. Asia Commun. Photon. Conf.*, Nov. 2016, paper AS1C.2.

[11] T. Jiang, C. Ni, C. Ye, Y. Wu, and K. Luo, "A novel multi-block tone reservation scheme for papr reduction in oqam-ofdm systems," *IEEE Trans. Broadcasting*, vol. 61, no. 4, pp. 717–722, Dec. 2015.

[12] E. Udayakumar and P. Vetrivelan, "PAPR reduction for OQAM/OFDM signals using optimized iterative clipping and filtering technique," in *Proc. Int. Conf. Soft-Comput. Netw. Secur.*, 2015, pp. 1–6.

[13] Y. Yoffe and D. Sadot, "Novel low resolution ADC-DSP optimization based on non-uniform quantization and MLSE for data centers interconnects," *Opt. Express*, vol. 24, no. 5, pp. 5346–5354, 2016.
[14] J. Peng, L. Han, Q. Zhu, C. Qiu, Y. Zhang, and C. Tremblay, "SQNR improvement enabled by nonuniform DAC output levels for IM-DD OFDM systems," *IEEE Photon. J.*, vol. 9, no. 2, Apr. 2017, Art. no. 7200411.
[15] T. Huang, M. Bi, G. Yang, L. Liu, X. Miao, H. Hao, S. Xiao, and W. Hu, "Nonuniform quantization DAC for improving the performance of IMDD-based FBMC system," in *Proc. Int. Conf. Opt. Commun. Netw.*, Aug. 2017, pp. 1–3.
[16] M. Bi, L. Zhang, L. Liu, G. Yang, R. Zeng, and S. Xiao, "Experimental demonstration of the OQAM-OFDM-based wavelength stacked passive optical networks," *Opt. Commun.*, vol. 394, pp. 129–134, 2017.
[17] C. Van Loan, *Computational Frameworks for the Fast Fourier Transform*. Philadelphia, PA, USA: SIAM, 1992.
[18] C. R. Berger, Y. Benlachtar, R. I. Killey, and P. A. Milder, "Theoretical and experimental evaluation of clipping and quantization noise for optical OFDM Theoretical and experimental evaluation of clipping and quantization noise for optical OFDM," *Opt. Express*, vol. 19, no. 18, pp. 17713–17728, Aug. 2011.
[19] K. Zheng and L. Shang, "High-linearity refractive index sensor based on analyte-filled defect hollow core bragg fiber," *IEEE Photon. Technol. Lett.*, vol. 29, no. 16, pp. 1391–1394, Aug. 2017.
[20] Q. Y. Yu, J. C. Guo, S. Y. Gao, W. X. Meng, and W. Xiang, "Minimum sum-mean-square-error frequency-domain pre-coding for downlink multi-user MIMO System in the frequency-selective fading channel," *IEEE Trans. Wireless Commun.*, vol. 16, no. 6, pp. 3753–3589, Jun. 2017.
[21] Q. Liu, X. Wang, N. S. V. Rao, K. Brigham, and B. V. K. V. Kumar, "Effect of retransmission and retrodiction on estimation and fusion in long-haul sensor networks," *IEEE/ACM Trans. Netw.*, vol. 24, no. 1, pp. 449–461, Feb. 2016.
[22] R. Bouziane *et al.*, "Optimizing FFT precision in optical OFDM transceivers," *IEEE Photon. Technol. Lett.*, vol. 23, no. 20, pp. 1550–1552, Oct. 2011.
[23] M. Bi, S. Xiao, H. He, J. Li, L. Liu, and W. Hu, "Power budget improved symmetric 40-gb/s long reach stacked wdm-ofdm-pon system based on single tunable optical filter," *IEEE Photon. J.*, vol. 6, no. 2, Apr. 2014, Art. no. 7900708.